Central European Journal of Energetic Materials
ISSN 1733-7178; e-ISSN 2353-1843

Cent. Eur. J. Energ. Mater. 2019, *16*(4): 547-563; DOI 10.22211/cejem/113123
Article is available in PDF-format, in colour, at:
http://www.wydawnictwa.ipo.waw.pl/cejem/Vol-16-Number-4-2019/CEJEM_00963.pdf

Research paper

Crystal Structure and Thermal Behaviour of Imidazolium 2,4,5-Trinitroimidazolate

Chen Jian[1], **Lian Pengbao**[1], **Chen Lizhen**[1], **Wang Jianlong**[1,*], **Chen Jun**[2]

[1] *School of Chemical Engineering and Technology, North University of China, 030051 Taiyuan, Shanxi, China*
[2] *Oriental Chemical Co., Ltd., 441403 Xiangyang, Hubei, China*
**E-mail:* 619379961@qq.com

Abstract: In this work, imidazolium 2,4,5-trinitroimidazolate was obtained from 2,4,5-tri-iodoimidazole in a yield of 48%. Single-crystal X-ray diffraction analysis showed that this compound belongs to the triclinic crystal system with space group P-1. Thermogravimetric-differential scanning calorimetry (TG-DSC) was performed under a nitrogen atmosphere at heating rates of 5, 10, 15 and 20 °C·min^{-1}. Compound 3 clearly exhibits an exothermic decomposition. The activation energy (E) and pre-exponential factor ($\ln A$) calculated by the Kissinger method were 113.67 kJ·mol^{-1} and 25.30 s^{-1}, respectively. The E values obtained by the FWO and KAS methods changed slightly from 103.33 to 113.69 kJ·mol^{-1} and from 101.52 to 111.97 kJ·mol^{-1}, respectively, which makes us believe that its thermal decomposition can be described using only one reaction model. The Šatava-Šesták method and the compensation effect were used to study the thermal decomposition mechanism of imidazolium 2,4,5-trinitroimidazolate. $\frac{d\alpha}{dt} = (e^{24.15})\left(e^{-108410/RT}\right)\left(\frac{2}{3}\alpha^{-\frac{1}{2}}\right)$ is regarded as the most appropriate thermal decomposition kinetic equation. The impact sensitivity, friction sensitivity, detonation velocity and explosion pressure of imidazolium 2,4,5-trinitroimidazolate were 43 cm, 46%, 7056.9 m·s^{-1} and 1.9703 · 10^{10} Pa (ρ = 1.538 g·cm^{-3}), respectively. Imidazolium 2,4,5-trinitroimidazolate is incompatible with RDX, HMX, TKX-50 and CL-20.

Keywords: imidazolium 2,4,5-trinitroimidazolate, crystal structure, thermal decomposition, TG-DSC, model-free methods

Supporting Information (SI), *i.e.* kinetic model functions, crystallographic data, spectra of FTIR and ^{1}H and ^{13}C NMR, and HPLC, for compound 3, as well as DSC curves of single and mixture systems, are available at: http://www.wydawnictwa.ipo.waw.pl/cejem/Vol-16-Number-4-2019/CEJEM_00963_SI.pdf

Other supplementary data: CCDC-1583551 contains the supplementary crystallographic data for this paper. The data can be obtained free of charge from the Cambridge Crystallographic Data Centre.

1 Introduction

In the past, nitroimidazoles and their intermediates have been used as antitumor, antibacterial, antifungal, and antiviral drugs due to their potent biological activities [1, 2]. Recently, polynitroimidazoles have attracted considerable interest as energetic materials [3, 4], especially highly energetic materials [5]. Many articles have reported new synthetic methods, explosive properties and applications of nitroimidazole derived compounds [6-9]. 2,4,5-Trinitroimidazole (Scheme 1, compound 2) is one nitroimidazole derivative, but it is not stable enough to be isolated [10]. However, the salts of 2,4,5-trinitroimidazole are stable and can be isolated [11-13]. Imidazolium 2,4,5-trinitroimidazolate (Scheme 1, compound 3) is a high energy and insensitive energetic material [13]. A better understanding of the thermal behaviour of compound 3 is important practically for its applications. However, disappointingly, there has been no report on the thermal behaviour of compound 3. The present study provides the first description of methods for the solid state characterization and thermal analysis of compound 3. Compound 3 was characterized by Fourier transform infrared (FTIR) spectroscopy, ^{1}H and ^{13}C nuclear magnetic resonance (NMR) spectroscopy, elemental analysis, single-crystal X-ray diffraction (XRD) and thermal analysis. The explosive properties of compound 3 and its compatibility with known explosives were investigated. Finally, the thermal behaviour of compound 3 is discussed.

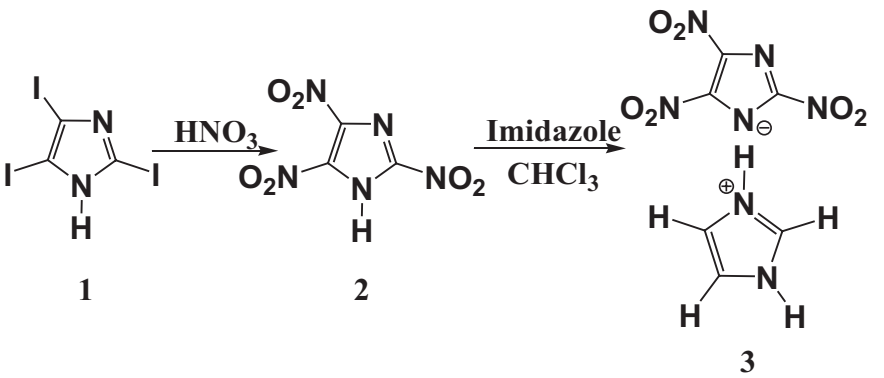

1 2 3

Scheme 1. Synthesis of imidazolium 2,4,5-trinitroimidazolate from 2,4,5-triiodoimidazole

2 Materials

All reagents, imidazole (AR, 99.5%), iodine (AR, 99.8%), potassium iodide (AR, 99.0%), nitric acid (AR, 98.0%), diethyl ether (AR, 99.5%), sodium bicarbonate (AR, 99.5%), anhydrous magnesium sulfate (AR, 99.5%), and chloroform (AR, 99.5%) were purchased from Xilong Scientific Co., Ltd. (Shanghai, China) and used without further purification.

3 Synthesis of Imidazolium 2,4,5-Trinitroimidazolate

2,4,5-Tri-iodoimidazole (Scheme 1, compound 1) was prepared as described previously [14]. Compound 1 (4.46 g, 0.01 mol) was added to 98% fuming nitric acid (60 mL) in an ice-water bath, and the mixture was heated to reflux temperature and stirred for 2.5 h, during which period a precipitate of iodic acid was deposited. Subsequently, the mixture was cooled to allow separation of the iodic acid precipitate, and the cooled mixture was then poured onto ice (200 g) and neutralized with saturated $NaHCO_3$ solution. The mixture was then extracted with diethyl ether (5 × 50 mL), the combined organic layers were washed with water, dried over $MgSO_4$ and filtered. Imidazole (0.68 g, 0.01 mol) dissolved in chloroform (10 mL) was added with stirring to the 2,4,5-trinitroimidazole (compound 2) as a diethyl ether solution, the precipitate was filtered off and recrystallized from water to yield a light yellow solid (compound 3), which was dried at 40 °C. The final yield

was 1.32 g (48.63%), and the purity was greater than 98.5% (see Scheme 1). HPLC of compound 3 is shown in Figure S1 (see SI).

Caution: Compound 3 is dangerous and thus caution should be exercised in handling and storage.

4 Test Methods

4.1 Single-crystal XRD analysis

The XRD patterns were recorded on a Bruker D8 VENTURE PHOTON100 CMOS diffractometer equipped with a graphite-monochromator and MoKα radiation (λ = 0.071073 nm). The structures were solved by direct methods (SHELXTL-2014/7 software) and refined by the full-matrix-block least-squares method on F2 with anisotropic thermal parameters for all non-hydrogen atoms [15]. The hydrogen atoms were added according to the theoretical models.

4.2 FTIR spectroscopy

The FTIR spectra were recorded from 400 to 3600 cm^{-1} at a resolution of 2 cm^{-1} on a Bruker Model Vertex 80 FTS spectrometer. A total of 32 scans were averaged into one spectrum using IR Solution software Opus6.5 (Bruker). Background spectra were recorded and subtracted during each analysis. The uniformity was verified at different locations of three samples.

4.3 ^{1}H and ^{13}C NMR spectroscopy

The ^{1}H and ^{13}C NMR spectra were recorded on a Bruker spectrometer with deuterated acetone as solvent at 400 and 100.58 MHz, respectively. The chemical shifts were reported in δ units [ppm] relative to TMS as an internal standard.

4.4 Elemental analysis

Elemental analyses were performed on an Elementar Vario EL elemental analyzer. The sample of approximately 1 mg was pyrolyzed with chromium oxide catalyst in an atmosphere of helium gas containing 3% oxygen. Carbon, hydrogen and nitrogen were converted into carbon dioxide, water, and nitrogen oxides, respectively. The nitrogen oxides were then converted to nitrogen by metallic copper reduction in a reduction furnace at 650 °C. Excess oxygen was absorbed by copper, and the nitrogen, carbon dioxide and water of the gas mixture were separated on a chromatographic column and detected by thermal conductivity. All analyses were performed in triplicate.

4.5 TG-DSC analysis

Thermogravimetric-differential scanning calorimetric TG-DSC analysis was carried out on a NETZSCH STA 409 PC/PG instrument. A sample of ~5 mg was placed in an alumina crucible and heated from 25 to 400 °C at heating rates of 5, 10, 15, or 20 °C·min^{-1} in a nitrogen atmosphere at a flow rate of 60 cm^3·min^{-1}. The TD-DSC test of the sample was carried out under open conditions. The data were analyzed using the Proteus software.

Non-isothermal data were analyzed using the model free Flynn-Wall-Ozawa (FWO) integral method [16], the Kissinger differential method [17] and the Kissinger-Akahira-Sonuse (KAS) differential method [18, 19]. The magnitude of the rate constant (k) was determined by the temperature (T) and was obtained from the Arrhenius equation [20]:

$$k = A\exp^{-E_a/RT} \tag{1}$$

where R is the gas constant [J·(K·mol)$^{-1}$], T is the temperature [K], A is the frequency factor, which is a constant describing the probability that a molecule with energy E will participate in the reaction, and E_a is the activation energy, which is also a constant describing the energy barrier opposing the reaction. A and E_a can be related to the conversion function $f(\alpha)$:

$$\frac{\mathrm{d}\alpha}{\mathrm{d}t} = A\exp^{\left(-E_a/RT\right)} f(\alpha) \tag{2}$$

Under isothermal conditions, Equation 2 becomes Equation 3.

$$\frac{\beta \mathrm{d}\alpha}{\mathrm{d}T} = A\exp^{\left(-E_a/RT\right)} f(\alpha) \tag{3}$$

where β is the heating rate [K·min^{-1}].

The FWO method [16] is based on the following equation:

$$\log\beta = \log\left[\frac{A_\alpha E_\alpha}{RG(\alpha)}\right] - 2.315 - 0.4567\frac{E_\alpha}{RT_\alpha} \tag{4}$$

The apparent activation energy can be obtained from the log(β) *vs*. $1/T_\alpha$ plot for a given value of conversion, α, where the slope is equal to $-E_\alpha/R$.

The Kissinger method [17] is described as follows:

$$\ln\left(\frac{\beta}{T_P^2}\right) = \ln\left[\frac{AR}{E}\right] - \frac{E}{RT_P} \tag{5}$$

where T_P is the peak temperature [K]. The apparent activation energy (E) and pre-exponential factor (A) can be obtained from the slope $-1/RT_P$ and intercept $\ln(AR/E)$ of the $\ln(\beta/(T_P)^2)$ *vs.* $1/T_P$ plot, respectively.

The KAS method is expressed as follows [18, 19]:

$$\ln\left(\frac{\beta}{T_\alpha^2}\right) = \ln\left[\frac{A_\alpha R}{E_\alpha G(\alpha)}\right] - \frac{E_\alpha}{RT_\alpha} \tag{6}$$

The apparent activation energy (E_α) can be obtained from the slope $-1/(RT_\alpha)$ of the $\ln(\beta/(T_\alpha)^2)$ *vs.* $1/T_\alpha$ plot.

4.6 Explosive properties and compatibility

The impact sensitivity was measured on a ZGT-2B instrument, with the drop hammer of 2.5 kg in the weight according to national military standard of the People›s Republic of China (GJB 772A-97). The weight of the sample was 35 mg.

The friction sensitivity measurement was performed on an MGY-2 pendulum friction sensitivity meter, according to national military standard of the People›s Republic of China (GJB 772A-97). The swing angle, vertical pressure, gauge pressure and sample weight were 90°, $5929 \cdot 10^5$ Pa, $49 \cdot 10^5$ Pa and 20 mg, respectively.

The detonation velocity (D) and explosion pressure (P_d) of the explosive samples were calculated using the Kamlet formulas. Equations 7 and 8 are the Kamlet formulas for detonation velocity and explosion pressure, respectively. Compatibility studies with well known explosives (RDX, HMX, TKX-50 and CL-20) were carried out on a NETZSCH DSC-214 apparatus. A sample of ~5 mg was placed in an alumina crucible and was heated from 25 to 350 °C at a heating rate of 10°C·min^{-1} in a nitrogen atmosphere at a flow rate of 60 mL·min^{-1}.

$$D = 0.7062\varphi^{1/2}(1 + 1.30\rho) \tag{7}$$

$$P_d = 7.617 \cdot 10^8 \varphi\rho^2 \qquad \varphi = NM^{1/2}Q^{1/2} \tag{8}$$

where D is the detonation velocity [km·s^{-1}] of the explosive when the filling density of the explosive is ρ [g·cm^{-3}], P_d is the C-J explosive pressure of the explosive [Pa], N is the mass of gaseous product produced per gram of explosive, M is the average molar mass of the gaseous detonation products,

φ is the characteristic value of the explosive, and Q is the heat of explosion per unit mass [J/g].

5 Results and Discussion

5.1 Single-crystal XRD patterns

Compound 3 crystallizes in the triclinic crystal system with space group P-1, and each elementary cell contains four molecules (crystallographic data are shown in Tables S1 to S4, in SI). The main crystallographic data are listed in Table 1. The compound exhibits an unsymmetrical structure, as shown in Figure 1.

Table 1. Crystal data and structure refinement for compound 3

Item	Value
Empirical formula	$C_6H_7N_7O_6$
Formula mass	271.17
Temperature [K]	173 ±2
Crystal system	triclinic
Crystal size [mm^3]	0.31 × 0.18 × 0.15
Space group	P-1
a [Å]	8.5859 ±0.0006
b [Å]	9.8010 ±0.0006
c [Å]	13.8029 ±0.0008
α [°]	69.760 ±0.002
β [°]	77.652±0.002
γ [°]	76.772 ±0.002
V [Å^3], Z	1049.29 ±0.12, 4
D_C [g cm^{-3}]	1.717
μ [mm^{-1}]	0.154
F(000)	552.0
θ [°]	5.794~50.742
h, k, and l range	–10~10, –11~10, –16~16
independent reflection (R_{int})	3844 (0.0539)
goodness-of-fit on F^2	1.035
R_1, wR_2 [$I > 2\sigma(I)$]	0.0449, 0.0863
R_1, wR_2 (all data)[a]	0.0814, 0.0980
$\Delta\rho_{max}$, $\Delta\rho_{min}$ [e Å^{-3}][a]	0.34, –0.32

[a] $w=1/[\sigma^2(F_o)^2 + (0.0430P)^2 + 0.1472P]$, where $P = ((F_o)^2 + 2(F_c)^2)/3$

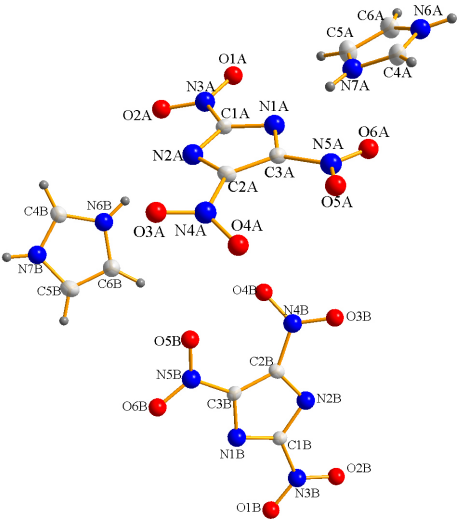

Figure 1. Molecular structure of compound 3 according to XRD analysis

The 2,4,5-trinitroimidazolate anion and imidazolium cation are not planar, which was verified by planes 1 and 2 [C(1A)–N(1A)–C(3A)–C(2A)–N(2A) and C(4A)–N(7A)–C(5A)–C(6A)–N(6A)] and planes 3 and 4 [C(1B)–N(1B)–C(3B)–C(2B)–N(2B) and C(4B)–N(7B)–C(5B)–C(6B)–N(6B)] exhibiting dihedral angles of 20.8° and 14.6°, respectively. The nitrogen atoms of the nitro groups lie in the plane of the imidazole ring, which is clearly shown by the N(3A)–C(1A)–N(2A)–C(2A), N(4A)–C(2A)–N(2A)–C(1A), N(5A)–C(3A)–N(1A)–C(1A), N(3B)–C(1B)–N(2B)–C(2B), N(4B)–C(2B)–N(2B)–C(1B), and N(5B)–C(3B)–N(1B)–C(1B) torsion angles of 178.2°, 177.0°, 179.7°, 177.9°, –177.7° and –175.4°, respectively. However, the oxygen atoms are twisted out of the plane. Compound 3 displays a conjugative effect in the imidazole ring; the bond lengths can be seen in Table S2 (see SI). This conjugative effect can also be found in compound 1 [21].

In the unit cell of compound 3, two 2,4,5-trinitroimidazolate anions are linked with four imidazolium cations by eleven hydrogen bonds (Figure 2 and Table 2), resulting in the formation of a two-dimensional infinite chain. It is noted that each chain is independent with no hydrogen bonding interactions between the chains, and it is the van der Waals forces that lead to the stable three-dimensional packing of the crystal. Compound 3 may be more stable than compound 2 due to the hydrogen bonds.

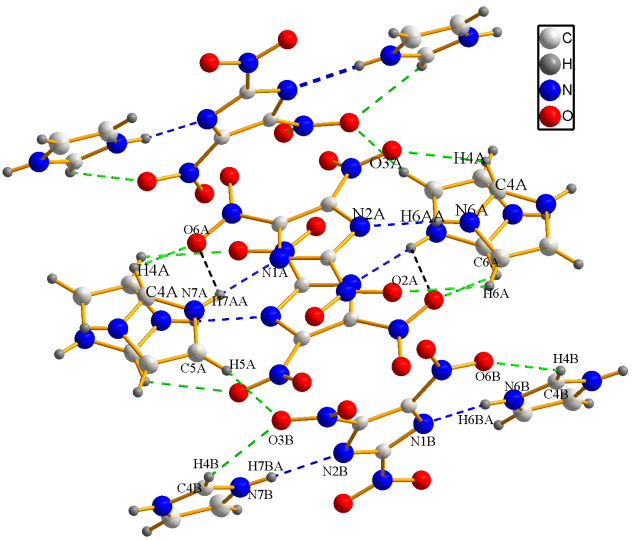

Figure 2. The 2D chains of compound 3 molecules

Table 2. Characteristics of the hydrogen bonds in the crystal structure of compound 3

D–H…A	d(D–H), [Å]	d(H···A), [Å]	d(D···A), [Å]	<(DHA), [deg]	Symmetry transformations
N(6A)–H(6AA)…N(2A)	0.8714	2.0092	2.878	174.453	x, 1+y, z
N(7A)–H(7AA)…N(1A)	0.8640	1.9839	2.8469	176.643	–
N(7A)–H(7AA)…O(6A)	0.8640	2.6478	3.1114	114.862	–
N(6B)–H(6BA)…N(1B)	0.8699	2.0430	2.070	172.025	–1+x, y, z
N(7B)–H(7BA)…N(2B)	0.8747	2.0502	2.9240	176.990	x, –1+y, z
C(4A)–H(4A)…O(3A)	0.9502	2.5220	3.1176	120.821	x, 1+y, z
C(4A)–H(4A)…O(6A)	0.9502	2.6178	3.1018	112.023	–
C(5A)–H(5A)…O(3B)	0.9496	2.5293	3.4057	153.551	–1+x, y, z
C(6A)–H(6A)…O(2A)	0.9496	2.6369	3.2003	118.463	x, 1+y, z
C(4B)–H(4B)…O(3B)	0.9502	2.5264	3.1500	123.315	x, –1+y, z
C(4B)–H(4B)…O(6B)	0.9502	2.5206	3.1043	119.789	–1+x, y, z

5.2 FTIR spectra

The IR spectra showed strong absorption peaks at 3146.4 and 2983.5 cm^{-1}, which can be attributed to the stretching vibration absorptions of C–H on the ring. The peaks at 1540.3 cm^{-1} and 1330.5 cm^{-1} were attributed to the asymmetric and symmetric stretching vibrations of C–NO_2, respectively, while those

at 1587.5 cm^{-1} and 1386.2 cm^{-1} were attributed to the stretching vibration absorptions of C=C and C=N, respectively, whose absorption peaks range from 1610 cm^{-1} to 1375 cm^{-1} (see Figure S2 in SI).

5.3 ^{1}H and ^{13}C NMR spectra

The ^{1}H NMR spectra (see Figure S3 in SI) obtained for compound 3 exhibited two chemical shifts, one at δ = 9.05 (1H) corresponding to the hydrogen of N=CH–N, and one at δ = 7.74 (2H) corresponding to the hydrogens of N–CH=CH–N. The N–H bond is too active to be detected. ^{13}C NMR spectrum (acetone-d_6), δ, ppm: 151.4, 144.1, 139.3, 130.2, 120.8, 118.5 (see Figure S4 in SI).

5.4 Elemental analysis

The elemental analysis showed that compound 3 is composed of C 26.69%, H 1.93%, and N 36.02%, while the calculated result for $C_6H_5N_7O_6$ is C 26.58%, H 1.86%, and N 36.16%.

5.5 TG-DSC curves

The TG-DSC curves of compound 3 at different heating rates under a N_2 atmosphere are shown in Figure 3. Clearly, compound 3 has only one obvious exothermic decomposition stage.

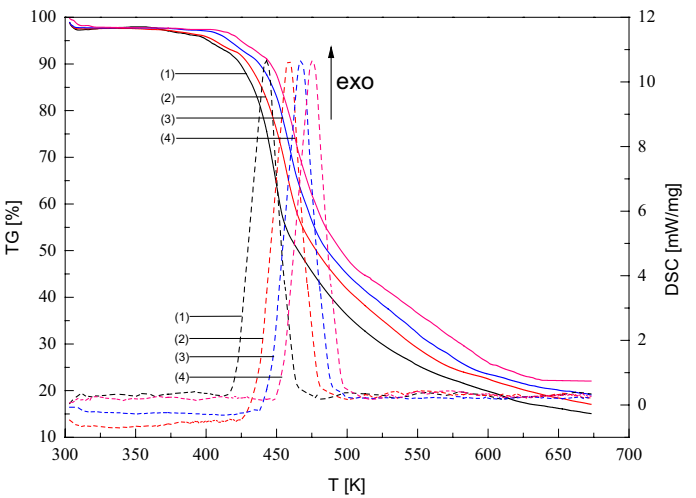

Figure 3. TG-DSC curves for compound 3 at different heating rates: (1) 5, (2) 10, (3) 15, (4) 20 °C·min^{-1}

The characteristic temperatures and weight losses in the TG-DSC curves are listed in Table 3. It shows that at 5 °C·min^{-1}, the extrapolated initial temperature (T_i) was 372.55 K, the peak temperature (T_p) was 448.95 K, the final temperature (T_f) was 425.75 K, and the decomposition enthalpy (ΔH) was 191.4 J·g^{-1}. The Kissinger method (Equation 5) was used to calculate the kinetic parameters (E and A) of the main exothermic decomposition reactions of compound 3. The E and ln$A$ values were 113.67 kJ·mol^{-1} and 25.30 s^{-1} for decomposition, respectively, as shown in Table 4. It also shows that the correlation coefficient (r^2) was very close to 1, indicating that kinetic parameters of high accuracy were obtained.

Table 3. Characteristic temperatures and weight losses in the TG-DSC curves of compound 3

β [°C min^{-1}]	T_i [K]	T_p [K]	T_f [K]	Weight loss [%]
5	372.55	448.95	625.75	79.71
10	380.95	457.75	628.95	76.78
15	397.45	463.95	633.45	76.44
20	406.15	469.05	638.35	75.09

Table 4. The E and ln$A$ values for the thermal decomposition of compound 3 obtained by the Kissinger method

E [kJ·mol^{-1}]	ln$A$ [s^{-1}]	r^2
113.67	25.30	0.9958

A major drawback of the Kissinger method is that it produces a single value for the activation energy for any process regardless of its actual kinetic complexity. Considering the complex thermal decomposition of triazole salts, the FWO and KAS methods were also used to calculate the kinetic parameters of compound 3 according to Equations 4 and 6, respectively, and the results are listed in Table 5. This shows that the E values obtained by the FWO and KAS methods were in the range of 103.33-113.69 and 101.52-111.97 kJ·mol^{-1}, respectively, and that the calculated correlation coefficients (r^2) were high in all cases. Obviously, the E value changes greatly. ω [%] is a constructed function defined as the ratio of the difference between the maximum and minimum values of E to the average of E:

$$\omega = \frac{E_{max} - E_{min}}{E_{average}} \cdot 100\% \tag{9}$$

The ω values obtained by the FWO and KAS methods were 9.56 and 9.80%, respectively, indicating that there is only one decomposition mechanism for the decomposition process and the activation energy is independent of the degree of conversion [22]. The averages of E calculated by the FWO and KAS methods were 108.41 and 106.60 kJ·mol^{-1}, respectively, which are similar to that calculated by the Kissinger method (113.67 kJ·mol^{-1}). The small difference is assumed to result from the limitations of the method itself and errors in the calculation. It should be noted that the average obtained by the mathematical method has no physical meaning. If the reaction order of decomposition is assumed, the mechanism function can also be determined by the FWO and KAS methods [23, 24].

Table 5. E values for the thermal decomposition of compound 3 obtained by the FWO and KAS methods

α	FWO		KAS	
	E [kJ mol^{-1}]	r^2	E [kJ mol^{-1}]	r^2
0.10	103.33	0.9980	101.83	0.9977
0.15	104.61	0.9918	102.99	0.9906
0.20	104.60	0.9930	102.83	0.9919
0.25	105.80	0.9916	104.00	0.9903
0.30	107.13	0.9895	105.35	0.9879
0.35	109.05	0.9924	107.32	0.9913
0.40	110.67	0.9906	108.99	0.9893
0.45	111.71	0.9918	110.05	0.9906
0.50	113.24	0.9951	111.63	0.9944
0.55	110.69	0.9964	108.90	0.9958
0.60	113.45	0.9929	111.78	0.9919
0.65	113.12	0.9934	111.40	0.9924
0.70	113.69	0.9920	111.97	0.9909
0.75	109.83	0.9905	107.89	0.9890
0.80	103.78	0.9914	101.52	0.9900
0.85	103.90	0.9925	101.60	0.9913
0.90	104.48	0.9977	102.18	0.9973
Average	108.41	–	106.60	–

Sometimes, the reaction model and pre-exponential factor (A) are determined by combining the results of a model-free method and some methods that involve model-fitting of single heating rate data. However, the reaction model and A are not determined by this model due to its methodological flaws.

Firstly, the single heating rate model-fitting value of E_1 rarely matches the model-free value of E with good accuracy. Secondly, it is common that two or more different $f(\alpha)$ or $G(\alpha)$ values yield E_1 values that fit within the confidence limits for E. Thirdly, for the same reaction model, the E and A values tend to change with the heating rate. All of these factors result in an inaccurate determination of the reaction models and pre-exponential factors (A).

The compensation effect can be made use of to establish the reaction model to avoid the flaws of model-fitting methods based on a single heating rate. The Šatava-Šesták method is a model fitting method, which was used to obtain E and A based on a heating rate of 5 °C·min^{-1}, then the expression of the kinetic compensation effect can be described as Equation 10:

$$lnA = 0.2061E + 1.8953 \tag{10}$$

Equation 11 can be obtained by converting Equation 2. Once both E and A have been determined, the reaction model can be establishedby plotting the calculated $f(\alpha)$ values against the theoretical $f(\alpha)$ values and finding the one that matches best [25].

$$f(\alpha) = \left(\frac{d\alpha}{dt}\right)_{\alpha} \left[Ae^{\left(\frac{-E}{RT_{\alpha}}\right)}\right]^{-1} \tag{11}$$

As mentioned earlier, the variation of E with degree of conversion seems to be negligible in the decomposition process here, so that the value of E in Equation 11 can be replaced with an average value of E obtained above by the KAS or FWO methods. The value of A can be calculated according to Equation 10. Thirty-nine forms of the kinetic model function are listed in Table S5 (see SI) [26].

The result is shown in Figure 4. From Figure 4, we can observe that the calculated $f(\alpha)$ values are on the whole consistent with the theoretical correlation obtained by the $f_{26}(\alpha)$ equation. So the $f_{26}(\alpha)$ equation is reasonable considering the differential form of the reaction model for the decomposition process of compound 3. The physical meaning of this model is the Mampel power mechanism (n = 3/2). The dynamic equation for the decomposition process of compound 3 is proposed as Equation 12:

$$\frac{d\alpha}{dt} = (e^{24.15})\left(e^{-108410/RT}\right)\left(\frac{2}{3}\alpha^{-\frac{1}{2}}\right) \tag{12}$$

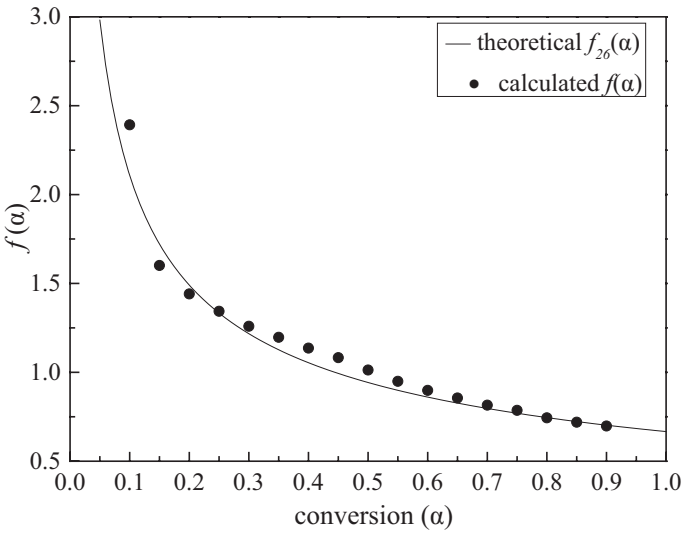

Figure 4. The calculated $f(\alpha)$ plot at different conversions in the decomposition process of compound 3

5.6 Explosive properties and compatibility

The impact sensitivity, friction sensitivity, detonation velocity and explosion pressure of compound 3 were 43 cm, 46%, 7056.9 m·s^{-1} and 1.9703 · 10^{10} Pa (ρ = 1.538 g·cm^{-3}), respectively. Compound 3 is incompatible with RDX, HMX, TKX-50 and CL-20, perhaps because compound 3 is an all-organic energetic ionic salt. The results are listed in Table 6. For DSC curves of single and mixture systems see Figure S5 (see SI).

Table 6. Data for binary systems obtained by DSC

Mixed system[a]	T_{p2} [K][b]	Single system[c]	T_{p1} [K][d]	ΔT_p [K][e]
compound 3/TKX-50	532.25	TKX-50	512.35	–19.90
compound 3/RDX	463.25	compound 3	459.55	–3.70
compound 3/HMX	547.75			–88.20
compound 3/CL-20	428.75			30.80

[a] Mixed system; compound 3/energetic component binary system, 50:50.
[b] T_{p2}, maximum exothermic peak temperature of the mixed system.
[c] Single system; component with an exothermic peak temperature lower than any other in a two-component system.
[d] T_{p1}, maximum exothermic peak temperature of the single system.
[e] $\Delta T_p = T_{p1} - T_{p2}$.

6 Conclusions

The main purpose of this study was to investigate the thermal behaviour of imidazolium 2,4,5-trinitroimidazolate. Single-crystal XRD analysis showed that imidazolium 2,4,5-trinitroimidazolate belongs to the triclinic crystal system with space group P-1. TG-DSC exhibited an exothermic decomposition. Kinetic parameters, such as apparent activation energy (E) and pre-exponential factor ($\ln A$), were obtained by model-free methods, including the Kissinger, FWO and KAS methods. The E and $\ln A$ values obtained by the Kissinger method were 113.67 kJ mol^{-1} and 25.30 s^{-1}. Unlike the Kissinger method, E from isoconversional methods was greatly dependent on the degree of conversion. Thus isoconversional methods are more efficient in revealing the decomposition mechanism compared to the Kissinger method. The E value obtained by the FWO and KAS methods changes slightly from 103.33 to 113.69 kJ mol^{-1} and from 101.52 to 111.97 kJ mol^{-1}, respectively, which makes us believe that its thermal decomposition can be described using only one reaction model, $f_{26}(\alpha)$, expressed as:

$$f_{26}(\alpha) = \frac{2}{3}\alpha^{-\frac{1}{2}}$$

The $f_{26}(\alpha)$ reaction model was established to be the differential form of the reaction model for the thermal decomposition process, by making use of the kinetic compensation effect, and the physical meaning underlying this model is the Mampel power mechanism (n = 3/2). The thermal decomposition kinetic equation of compound 3 can be expressed as:

$$\frac{d\alpha}{dt} = (e^{24.15})\left(e^{-108410/RT}\right)\left(\frac{2}{3}\alpha^{-\frac{1}{2}}\right)$$

The impact sensitivity, friction sensitivity, detonation velocity and explosion pressure of compound 3 were 43 cm, 46%, 7056.9 m·s^{-1} and 1.9703 · 10^{10} Pa (ρ = 1.538 g·cm^{-3}), respectively. Compound 3 was found to be incompatible with RDX, HMX, TKX-50 and CL-20.

Acknowledgements

We thank the Center of Testing and Analysis, Beijing University of Chemical Technology, for support.

References

[1] Breccia, A.; Cavalleri, B.; Adams, G.E. *Nitroimidazoles: Chemistry, Pharmacology and Clinical Applications.* Springer, New York, **1982**, pp. 15-18; ISBN 978-0-387-98069-0.

[2] Crozet, M.D.; Remusat, V.; Curti, C.; Vanelle, P. Rapid Synthesis of New 5-Nitroimidazoles as Potential Antibacterial Drugs *via* VNS Procedure. *Synth. Commun*. **2007**, *38*: 3639-3646.

[3] Bulusu, S.; Damavarapu, R.; Autera, J.R.; Behrens, R.J.; Minier, L.M. Thermal Rearrangement of 1,4-Dinitroimidazole to 2,4-Dinitroimidazole: Characterization and Investigation of the Mechanism by Mass Spectrometry and Isotope Labeling. *J. Phys. Chem.* **1995**, *99*: 5009-5015.

[4] Rice, B.M.; Hare, J.J. A Quantum Mechanical Investigation of the Relation Between Impact Sensitivity and the Charge Distribution in Energetic Molecules. *J. Phys. Chem. A.* **2002**, *106*: 1770-1783.

[5] Badgujar, D.M.; Talawar, M.B.; Mahulikar, P.P. Review of Promising Insensitive Energetic Materials. *Cent. Eur. J. Energ. Mater.* **2017**, *14*(4): 821-843.

[6] Szala, M.; Lewczuk, R. New Synthetic Methods for 4,4',5,5'-Tetranitro-2,2'-bi-1*H*-imidazole (TNBI). *Cent. Eur. J. Energ. Mater.* **2015**, *12*(2): 261-270.

[7] Lewczuk, R.; Szala, M.; Rećko, J.; Cudziło, S.; Klapotke, T.M.; Trzciński, W.A.; Szymańczyk, L. Explosive Properties of 4,4',5,5'-Tetranitro-2,2'-bi-1*H*-imidazole Dihydrate. *Cent. Eur. J. Energ. Mater.* **2016**, *13*(3): 612-626.

[8] Bogusz, R.; Rećko, J.; Magnuszewska, P.; Lewczuk, R. Application of the Energetic Complex $[Cu(TNBI)(NH_3)_2(H_2O)]$ in Heterogeneous Solid Rocket Propellants. *Cent. Eur. J. Energ. Mater.* **2018**, *15*(2): 391-402.

[9] Li, Y.N.; Shu, Y.J.; Wang, Y.L.; Wang, B.Z.; Zhang, S.Y.; Bi, F.Q. Synthesis, Structure and Energetic Properties of a Catenated N_6, Polynitro Compound: 1,1'-Azobis(3,5-dinitropyrazole). *Cent. Eur. J. Energ. Mater.* **2017**, *14*(2): 321-335.

[10] Cho, J.R.; Kim, K.J.; Cho, S.G.; Kim, J.K. Synthesis and Characterization of 1-Methyl-2,4,5-Trinitroimidazole(MTNI). *J. Heterocycl. Chem.* **2002**, *39*: 141-147.

[11] Novikov, S.S.; Khmel'nitskii, L.I.; Lebedev, O.V.; Sevost'yanova, V.V.; Epishina, L.V. Nitration of Imidazoles with Various Nitrating Agents. *Chem. Heterocycl. Compd.* **1970**, *6*: 465-469.

[12] Katritzky. A.R; Cundy, D.J; Chen, J. Polyiodoimidazoles and Their Nitration Products. *J. Energ. Mater.* **1993**, *11*: 345-352.

[13] Gao, H.X.; Ye, C.F.; Gupta, O.D.; Xiao, J.C.; Hiskey, M.A.; Twamley, B.; Shreeve, J.M. 2,4,5-Trinitroimidazole-Based Energetic Salts. *Chem. Eur. J.* **2007**, *13*: 3853-3860.

[14] Bmnings, K.J. Preparation and Properties of the Iodohistidines. *J. Am. Chem. Soc.* **1947**, *69*: 205-208.

[15] Sheldrick, G.M. A Short History of SHELX. *Acta Crystallogr. Sect. A.* **2008**, *64*: 112-114.

[16] Ozawa, T. A New Method Analyzing Thermogravimetric Data. *Bull. Chem. Soc. Jpn.* **1965**, *38*: 1881-1886.
[17] Kissinger, H.E. Reaction Kinetics in Differential Thermal Analysis. *J. Anal. Chem.* **1957**, *29*: 1702-1706.
[18] Kissinger, H.E. Variation of Peak Temperature with Heating Rate in Differential Thermal Analysis. *J. Res. Nat. Bur. Sta.* **1956**, *57*: 217-221.
[19] Akahira, T.; Sunose, T. Joint Convention of Four Electrical Institutes: Method of Determining Activation Deterioration Constant of Electrical Insulating Materials. *Res. Rep. Chiba Inst. Technol.* (*Sci. Technol.)* **1971**, *16*: 22-31.
[20] Brown, M.E.; Maciejewski, M.; Vyazovkin, S.; Nomen, R. Computational Aspects of Kinetic Analysis Part A: the ICTAC Kinetics Project-Data, Methods and Results. *Thermochim. Acta* **2000**, *355*: 125-143.
[21] Andrzejewski, M.; Marciniak, J.; Rajewski, K.W.; Katrusiak, A. Halogen and Hydrogen Bond Architectures in Switchable Chains of Di- and Trihaloimidazoles. *Cryst. Growth. Des.* **2015**, *15*(4): 1658-1665.
[22] Du, X.J.; Li, X.D.; Zou, M.S; Yang, R.J.; Pang, S.P.; Li, Y.C. Thermogravimetric Analysis and Kinetic Study of 1-Amino-1,2,3-Triazolium nitrate. *Thermochim. Acta* **2013**, *570*: 59-63.
[23] Slopiecka, K.; Bartocci, P.; Fantozzi, F. Thermogravimetric Analysis and Kinetic Study of Poplar Wood Pyrolysis. *Appl. Energy.* **2012**, *97*: 491-497.
[24] Chowdhury, A.; Thynell, S.T. Confined Rapid Thermolysis/FTIR/ToF Studies of Methylamino-triazolium-based Energetic Ionic Liquids. *Thermochim. Acta* **2010**, *505*: 33-40.
[25] Vyazovkin, S.; Burnham, A.K.; Criado, J.M.; Pérez-Maqueda, L.A.; Popescu, C.; Sbirrazzuoli, N. ICTAC Kinetics Committee Recommendations for Performing Kinetic Computations on Thermal Analysis Data. *Thermochim. Acta* **2011**, *520*: 1-19.
[26] Hu, R.Z.; Gao, S.L.; Zhao, F.Q.; Zhen, S.Q.; Zhang, T.L.; Zhang, J.J. *Thermoanalysis Kinetics.* (in Chinese) 2nd ed., Science Press, Beijing, **2008**, pp. 143-168; ISBN 978-7-03-020207-9.

Received: July 21, 2018
Revised: October 12, 2019
First published online: December 20, 2019